USGS Award Number: G13AP00069

Title: Using GPS Derived Shear Strain Rates in Southern California to Constrain Fault Slip Rate, Locking Depth, and Residual Off-Fault Strain Rates

William E. Holt
Dept. of Geosciences
Stony Brook University
Stony Brook, NY 11794-2100
Ph: 631 632-8215
Fax: 631 632-8240

Term: September 2013 through August 2014

Abstract

Strain rate fields within strike-slip regimes often possess complexity associated with along-strike slip rate variations. These along-strike slip rate variations produce dilatational components of strain rate within and near the fault zones and within the adjacent block areas. These dilatation rates do not directly reflect the slip rate magnitude on the strike slip fault, but rather the relative change in along-strike slip rate. Displacement rates measured using GPS observations reflect the full deformation gradient field, which may involve significant dilatational components together with other off-fault deformation. Thus, using displacement rates to infer slip rate and locking depth of major strike-slip faults may introduce errors when along-strike slip rate variations are present. On the contrary, the shape and magnitude of the shear strain rates (pure strike-slip component) reflect the true strike-slip parameters of interest (locking depth and slip rate). In this study we use of shear strain rates alone (obtained from the full displacement rate field of the SCEC 4.0 velocity field in southern California) to infer fault slip rate and locking depth parameters along the San Andreas (up to 37° N) as well as the San Jacinto fault zones. Such an analysis is critical for accurate estimation of off-fault strain rates outside of the major shear zones.

Results to date from this methodology applied to southern California using the SCEC 4.0 GPS velocity field, along with the UCERF3 GPS velocity field, show remarkably well-resolved and prominent shear strain rate bands that follow both the San Andreas and San Jacinto fault systems. The shear strain rates show evidence of dramatic along-strike slip rate variations. We obtain locking depths that are shallower than many previous estimates along several sections of the San Andreas system (e.g. Big Bend region). We hypothesize that contamination from off-fault strain rates can result in errors in fault locking depth and slip rate estimates. Our treatment of modeling only the shear strain rates acts as a ‘filter’ to remove signals in the displacement rate field that are unrelated to pure strike-slip deformation, thereby providing more accurate model estimates of slip rate and locking depth along these major strike-slip shear zones.

1.0 Method For Estimating Continuous Velocity Gradient Tensor Field from GPS

The methodology consists of interpolating velocities within a region to estimate the velocity gradient tensor field [e.g., *Holt et al*., 2000a, 2000b; *Beavan and Haines*, 2001]. These velocities are from the SCEC 4.0 velocity field. We have obtained a second solution from the UCERF3 GPS velocity field (Figures 1, 2). Regularization of the solution for Southern California consists of obtaining the sharpest estimate of strain tensor field possible that can be supported by the cGPS data. The smoothing of the strain solution is controlled through optimization of the following functional in a formal least-squares joint inversion of strain and displacement field:

$$\chi = \sum_{cells\, ij,kl}\sum (\hat{e}_{ij} - e_{ij}^{obs})^T \mathbf{V}_{ij,kl}^{-1} (\hat{e}_{kl} - e_{kl}^{obs}) + \sum_{knots\, i,j}\sum (\hat{u}_i - u_i^{obs})^T \mathbf{V}_{i,j}^{-1} (\hat{u}_j - u_j^{obs}), \qquad (1)$$

where $\mathbf{V}_{ij,kl}$ is the variance-covariance matrix of the strains, $\mathbf{V}_{i,j}$ is the variance-covariance of the displacements, $\hat{e}_{ij}$ and e_{ij}^{obs} are the model and observed strains, and $\hat{u}_i$ and u_i^{obs} are the model and observed displacements. The fitting algorithm that minimizes (1) is equivalent to a finite element method that satisfies force balance equations (spherical Earth). The methodology solves the Weak formulation of the linear problem, where the basis functions for the displacements are higher order elements involving the Bessel form of bi-cubic spline interpolation on a generally curvilinear grid of quadrilateral sub-domains [*de Boor*, 1978; *Beavan and Haines*, 2001] (0.1°x0.1° grid). The final model predicts a continuous displacement gradient tensor field (Figure 3). Finer grid spacing can be used to adapt to problems supported by dense station spacing. We use a constant Poisson's ratio of 0.25 and displacement boundary conditions may or may not be imposed. Also, *a priori* constraints from fault location, strike and expected range of fault slip rates can be used to define anisotropic and inhomogeneous components of the variance-covariance matrix $\mathbf{V}_{ij,kl}$, which influences the model parameter estimates for interpolated displacements and strains.

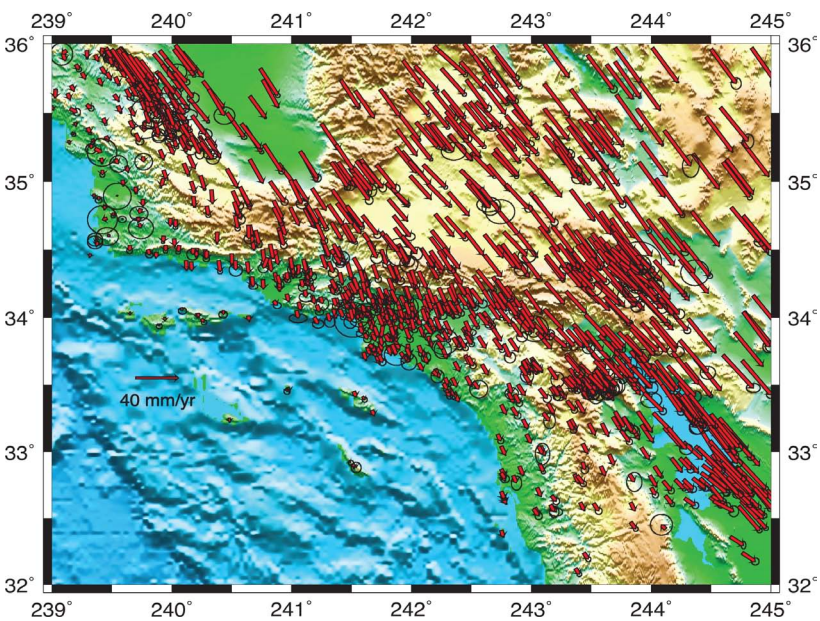

Figure 1. UCERF3 GPS Velocity field in a North American reference Frame.

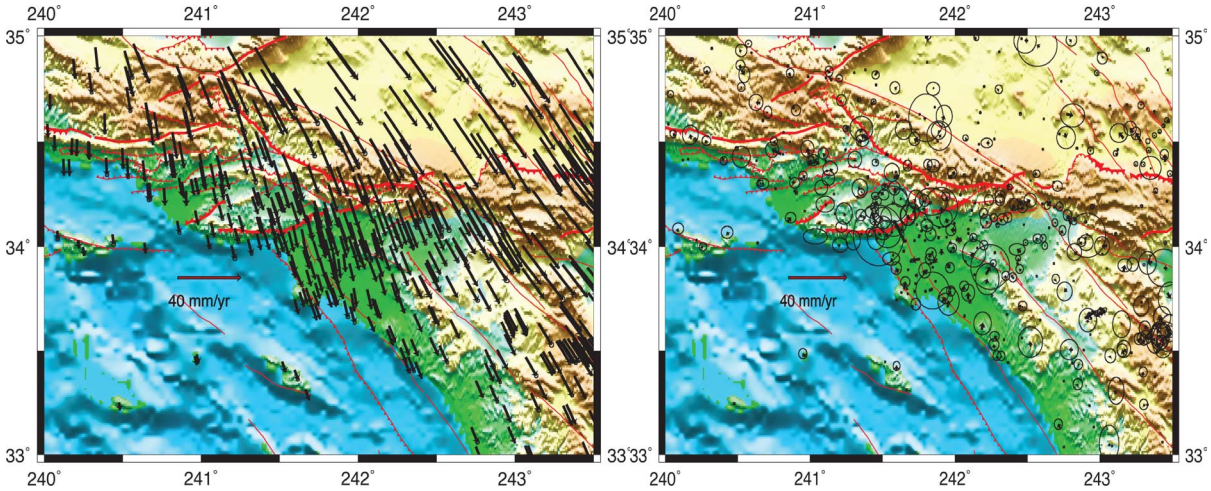

Figure 2. (Left). Model velocity from interpolation of UCERF3 velocity field in Figure 1. (Right) Residual velocities from observed minus predicted motions.

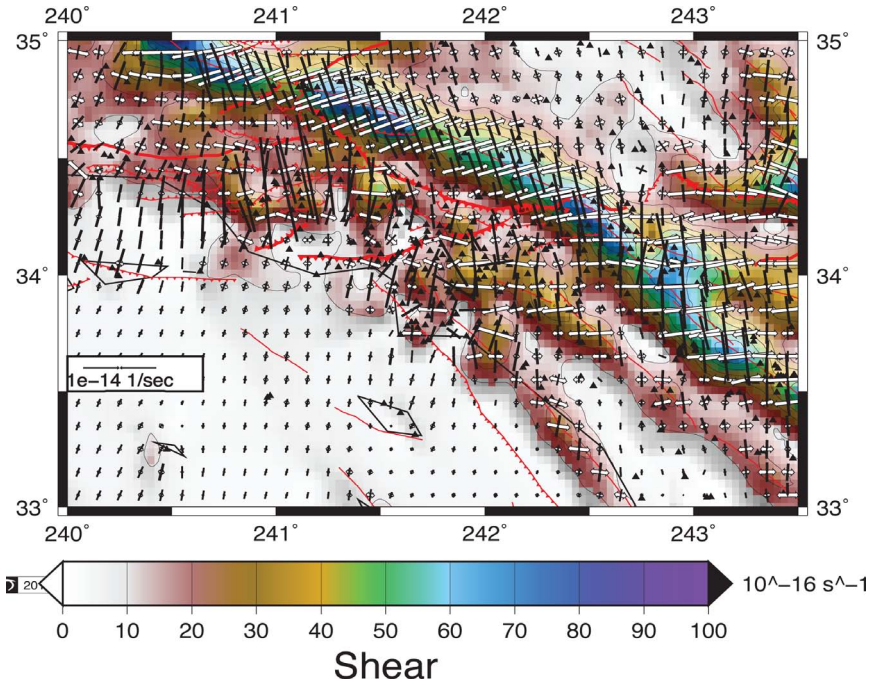

Figure 3. Principal axes of strain rate from model continuous strain rate tensor field obtained from interpolation of UCERF3 GPS velocity field (bold = compressional, open = extensional). The magnitudes of pure strike slip strain rates are contoured. We invert these shear strain rate magnitudes for fault locking depth and fault slip rate.

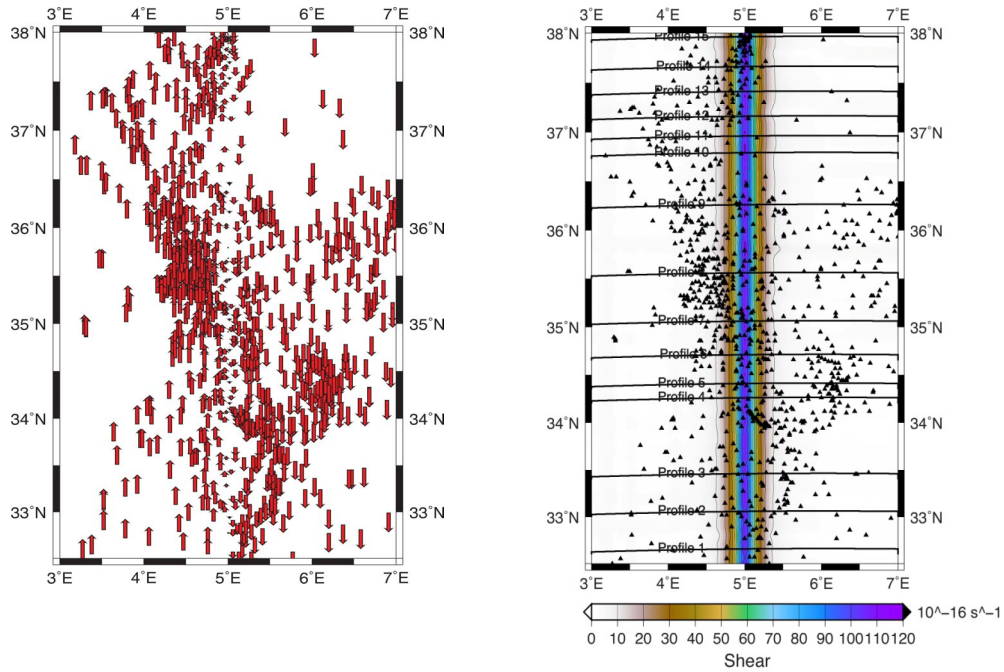

Figure 4: (left) Displacements output from Coulomb3.2 code for for a right-lateral fault slipping at 25 mm/yr with a locking depth of 10 km. (Right) Contoured shear strain rate magnitudes obtained from bi-cubic Bessel interpolation of displacements that were output from Coulomb code

2.0 Benchmarking Results Using Output from Okada's Elastic Dislocation Routine

We generated synthetic displacement fields using the code Coulomb 3.2 [*King et al*., 1994; *Lin and Stein*, 2004], an adaptation of *Okada* (1992). We output displacements at the same station spacing as the SCEC4.0 velocity field (Figure 4). For simplification we generated displacements for a single pure strike-slip fault that passed through the approximate centroid of the GPS station density. For the benchmarking exercise only, the synthetic fault was N-S oriented and thus the California stations were rotated about a point at about 32° S, 115°W, such that the distribution of stations that roughly follows the NW oriented trend of the plate boundary zone are now oriented N-S. A 0.1°x0.1° grid (same grid spacing used for Southern California) was used for the bi-cubic interpolation of the synthetic displacements. In this particular test case the longitude is arbitrary, and the fault was placed at a longitude of 5° (Figure 4). The variances and covariances of the strain rates (see equation 1) reflect the *a priori* expectation of a strike-slip fault in the region, with unknown slip rate magnitude. The shear strain rates, for a fault slipping at 25 mm/yr with a locking depth of 10 km, are shown in Figure 4 (right panel). The dilatational strain rates from this model, which should ideally be zero, varied between $\pm$ 0.25×10^{-16} s^{-1}, almost two orders of magnitude smaller than the magnitude of shear strain rate (120×10^{-16} s^{-1}). Therefore, the interpolation method that we employ (with anisotropic variance-covariances of strain rates) does

not show the strain rate artifacts that *Baxter et al*. [2010] described and found when they interpolated the present-day GPS station distribution in southern California.

2.1 Inversion of Shear Strain Rate Magnitudes for Fault Slip Rate and Fault Locking Depth

One simple step in our model interpretation will be to model 1-D profiles of shear strain rate using the simple screw dislocation of *Savage and Burford* [1973]. This, of course, is an approximation and an oversimplification because this 1-D treatment assumes that the fault possesses slip parameters an infinite distance along-strike; it is this assumption that we are attempting to move away from. However, the modeling of the full spatial distribution of velocities for the full horizontal velocity gradient tensor field already captures the along-strike variation in strain rate. The use of Savage and Burford treatment does not impose any limitation in our modeling. It only provides a simple and easily understood way to estimate point values of slip rate and locking depth within the model estimates of the true shear strain rate field in southern California.

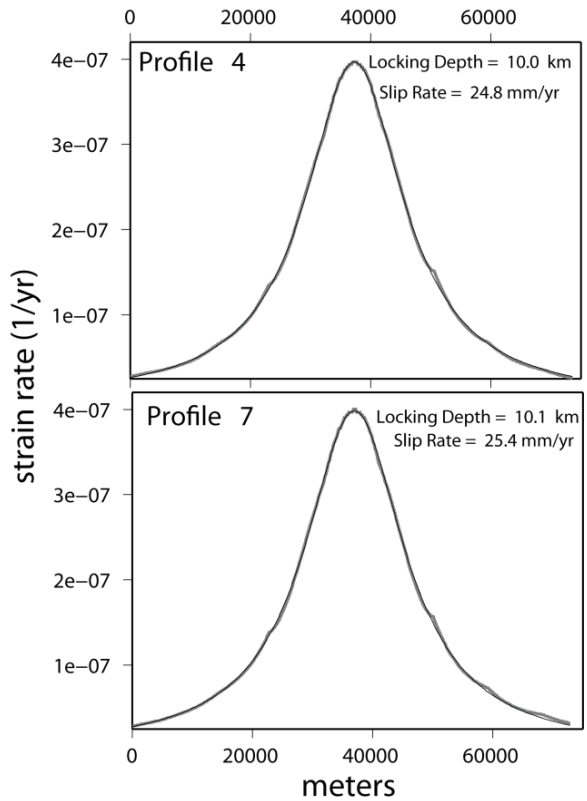

Figure 5. Selected profiles through the model shear strain rate field (gray line) along with the model fit to this profile from elastic screw dislocation model (*Savage and Burford*, 1973) (thin gray line). The screw dislocation model fit was obtained in a non-linear inversion for best-fit locking depth, slip rate, and fault location. The true parameters from the Okada – Coulomb 3.2 routine are 25 mm/yr and a locking depth of 10 km. The inversion routine also located the fault.

We invert profiles of shear strain rate, e_{xy}', using a conjugate gradient technique that minimizes the misfit between shear strain rates obtained from the strain rate model and those obtained from idealized *Savage and Burford* (1973) model (Figure 3). We solve for fault locking depth, fault slip rate, and fault location. Initially we test the method on the simple solution in Figure 2. Following this simple test, we test the method of recovering the velocity gradient tensor field and fault parameters using a dislocation model that possesses along-strike variation in slip rate. For the simple test in Figures 2 and 3, the misfit to the true model slip rates and locking depths (built into the Okada routine that generated the displacement rates) was not greater than 0.4 mm/yr and 0.5 km, respectively, for all 15 profiles.

2.2: *Benchmarking: Interpolation of displacement rates from a model with along-strike slip rate variations*

We next built a model using Coulomb 3.2 that has along-strike slip rate variations, but with constant fault locking depth of 10 km (Figure 6a,b). Slip rates are 16 mm/yr in the south. Slip rates transition to 23 mm/yr between 34°N and 34.6° N; rates transition to 30 mm/yr between 36.7°N and 37.3° N (Figure 6b). The variances and covariances of the strain rates again reflect

the *a priori* expectation of a strike-slip fault in the region, with unknown slip rate magnitude. The interpolation scheme reproduced the shear strain rate magnitudes (Figure 6a). Off-fault dilatation rates are prominent in the transition zone regions only, and are not present along sections of constant slip rate (Figure 5). There is, therefore, a minimum of dilatational strain rate artifacts. The off-fault dilatation rates between 34.0°N and 34.5°N are real features associated with the transition in slip rate. Strain rate tensor calculations are consistent throughout the region, reflecting accurate recovery of the true strain rate field through interpolation of the displacement rates with SCEC 4.0 station spacing (Figure 4).

Results from inversion of shear strain rates along the 15 profiles in Figure 6a are generally consistent with the true parameters (Figure 6b). Profiles 4, 5, 6 and 10, 11, and 12, within the transition zones in slip rate, show slightly larger misfits of order 1.5 mm/yr and 1 km for rate and locking depth, respectively.

In summary, we have found that interpolation of the GPS field (with station spacing equivalent to that found in the SCEC 4.0 velocity field) yields minimal dilatational strain rate artifacts, in contrast to the results of *Baxter et al*. [2010]. The anisotropic treatment of the variance-covariance matrix of the model rates of strain contributes to the stability to this problem.

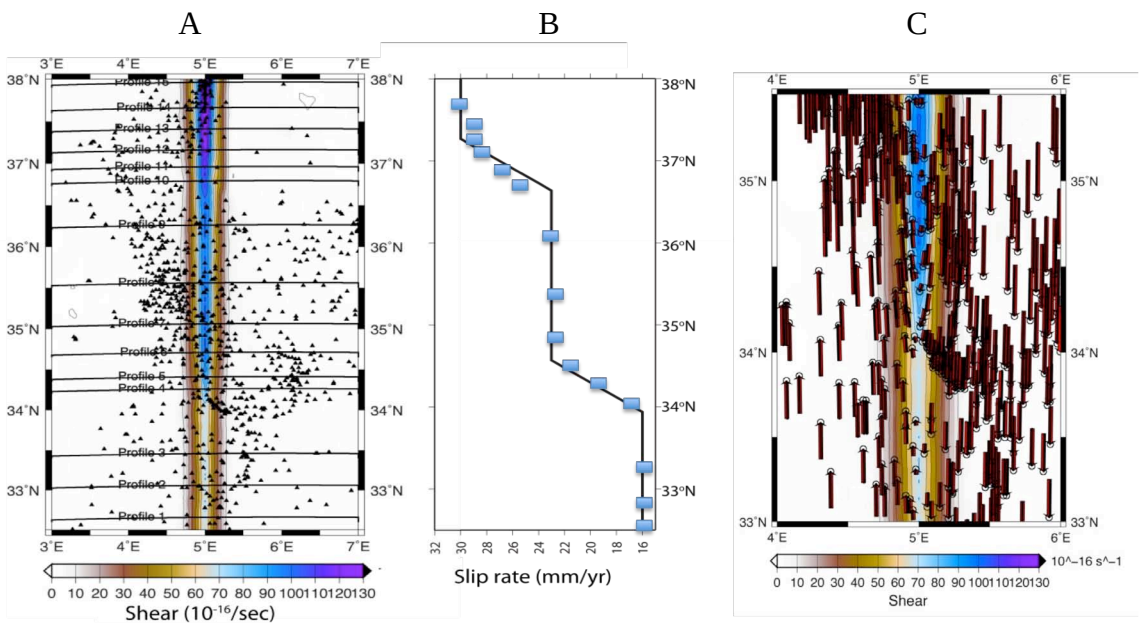

Figure 6. (A). Shear strain rate magnitudes obtained from bi-cubic interpolation of displacement rates generated using Coulomb 3.2, with slip rates that increased from south to north (locking depth 10 km). Displacement rate locations are shown by the triangles (which have the same spacing as in the SCEC 4.0 GPS velocity field. (B): Slip rate variation input into Coulomb (mm/yr) as a function of latitude, with inversion results (blue squares). Zones of transition are between 34 N and 34.5 N and between 36.6 N and 37.3 N. (C): Zoom-in on portion of displacements produced from the Coulomb code (RED) for fault with locking depth of 10 km and slip rate variation in Figure 6a. The errors for the displacement rates were assumed to be similar in size to the SCEC 4.0 GPS standard errors. The model fit to the GPS velocities from the bi-cubic spline interpolation is shown at the sites as black velocity vectors. Velocities are plotted on top of contoured magnitudes of shear strain rate.

3.0 Inversion Results

We have selected more than 100 profiles across the belts of prominent shear in the optimal strain rate solution obtained from the UCERF3 GPS velocity field. Using the method described in section 2 we inverted the shear strain rate distributions for slip rate and locking depth (Figure 7). For regions where faults are parallel to sub-parallel (San Jacinto and southern San Andreas) we set up codes to invert for two fault locking depths simultaneously. A general summary of results is shown in Figure 8.

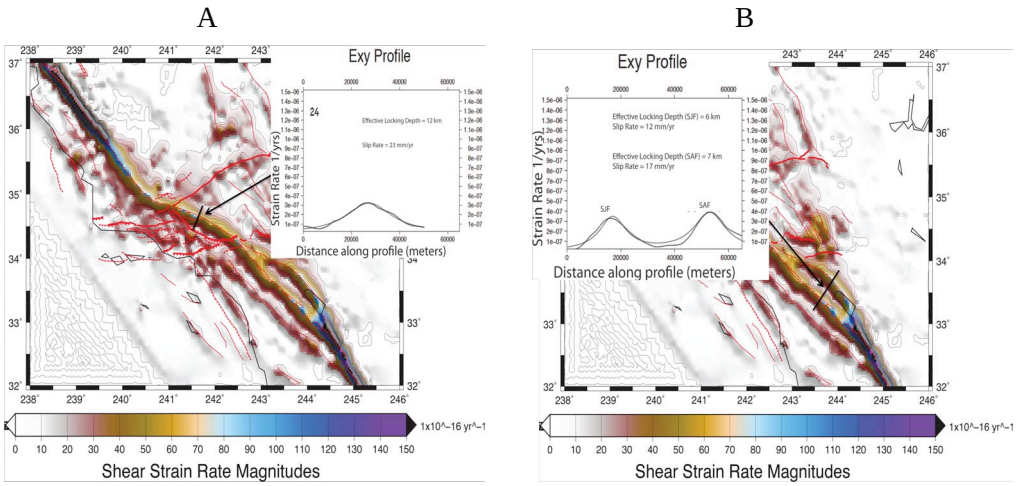

Figure 7. (A): Contoured shear strain rate magnitudes (associated with pure strike-slip faulting) and an example profile across the Mohave segment of the San Andreas within inversion results. The observed and predicted shear strain rate profiles are shown. In this example the locking depth was 12 km and the slip rate is 23 mm/yr. (B). Example of inversion result across the San Jacinto and San Andreas segments.

We obtain shallower effective locking depths (Figure 8) than previous studies. One possibility is that off-fault deformation, which is embedded in the total velocity field, contaminates estimates of the true signal associated with the pure strike slip structure. The method we employ effectively filters out deformation that is not associated with the major strike-slip structure. The isolation of pure strike-slip associated shear strain possibly allows a better estimate of both the slip rate and locking depth. Along strike variations are complex, and the disadvantage of inverting velocity profiles for slip rate and locking depth is that motions that are out of the plane, which are projected onto the 1-D plane, may bias results. Alternatively, the velocity gradient tensor field obtained from the GPS velocities satisfies compatibility equations at all points (an infinite number of line integrals across all possible paths across the plate boundary zone will give plate motion). Along strike variations embedded in the velocity field are accounted for and are reflected in the solution. Thus variations in slip rate and locking depth along strike will be reflected in the peak height and width of the shear zone. These same along strike variations will also be accommodated by considerable off-fault deformation. In a separate publication in preparation, we will provide full details of inversion results, including uncertainties, for all segments.

4.0 Off Fault Deformation Rates

Using the results obtained from the inversion of shear strain rates, together with the total velocity gradient tensor field obtained for the entire plate boundary zone, we estimate the budget of total deformation accommodated by off fault deformation. In order to calculate off-fault deformation we subtracted out the pure strike-slip deformation component associated with all major strike-slip faults. The Transverse Ranges in general do not involve strike-slip motions, but they were not counted in the budget for off fault deformation. We also determined the total tectonic moment rate within southern California (Figure 9). The minimum tectonic moment rate can be calculated using:

$$\dot{M}_o = 2\mu V(|\dot{\sigma}| + \sqrt{\dot{\gamma}_1^2 + \dot{\gamma}_2^2}), \qquad (2)$$

where μ is the shear modulus, V is the seismogenic volume, $\dot{\sigma}$ is the dilatation rate, $\dot{\gamma} = (\dot{\varepsilon}_{\phi\phi} - \dot{\varepsilon}_{\theta\theta})$ and $\dot{\gamma}_2 = \varepsilon_{\phi\theta}$. We obtain a total moment rate for the area shown in Figure 8 in Southern California of 2.2x10^{19} Nm/yr (Figure 9). A total of 6.6x10^{18} Nm/yr of tectonic moment rate is accommodated by off fault deformation. This is 30% of the total tectonic moment rate budget across the plate boundary zone in southern California.

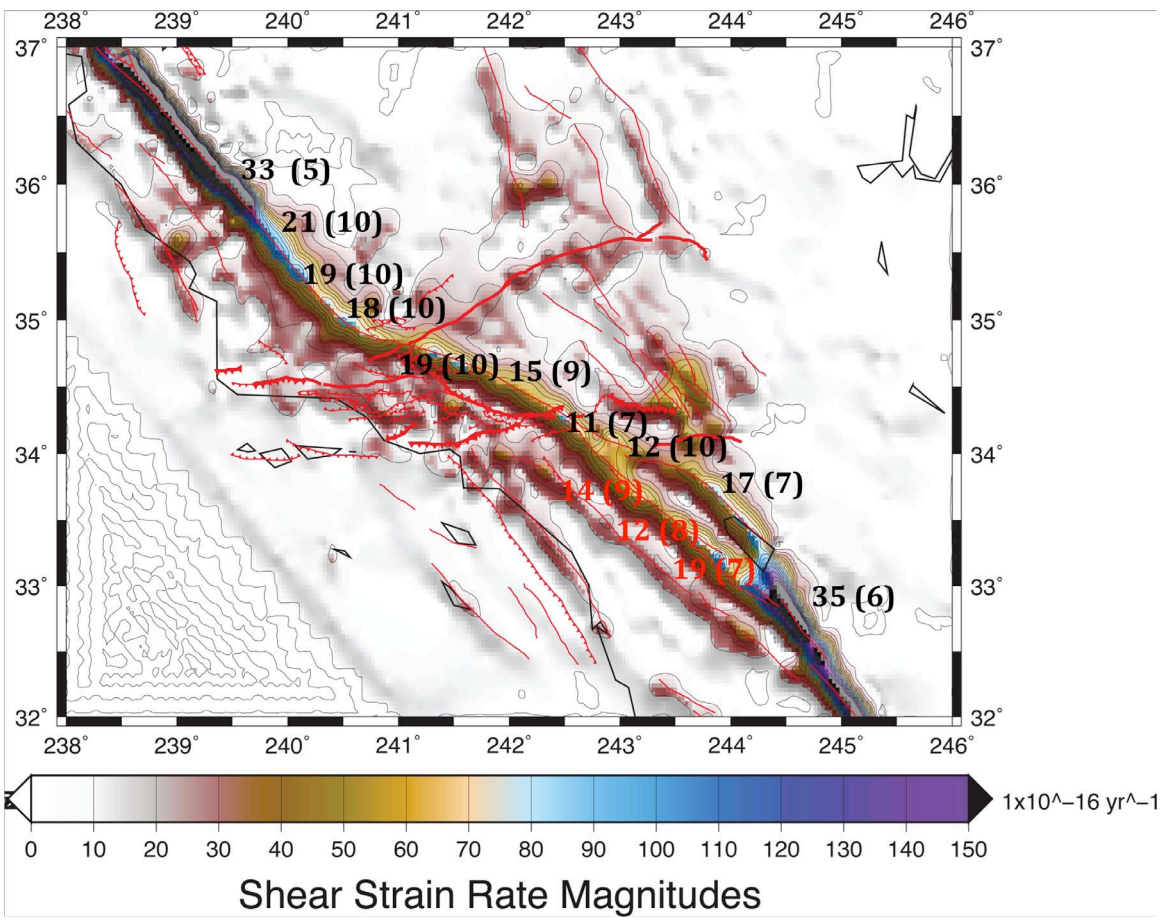

Figure 8. Summary of slip rates and locking depths (parentheses) obtained from inversion of shear strain rates. Several profiles within each segment were averaged to provide these summary values. Formal uncertainties are not shown, but are in the range of ±3 mm/yr for slip rate and ± 2 km for locking depth. Values in red are for the San Jacinto fault.

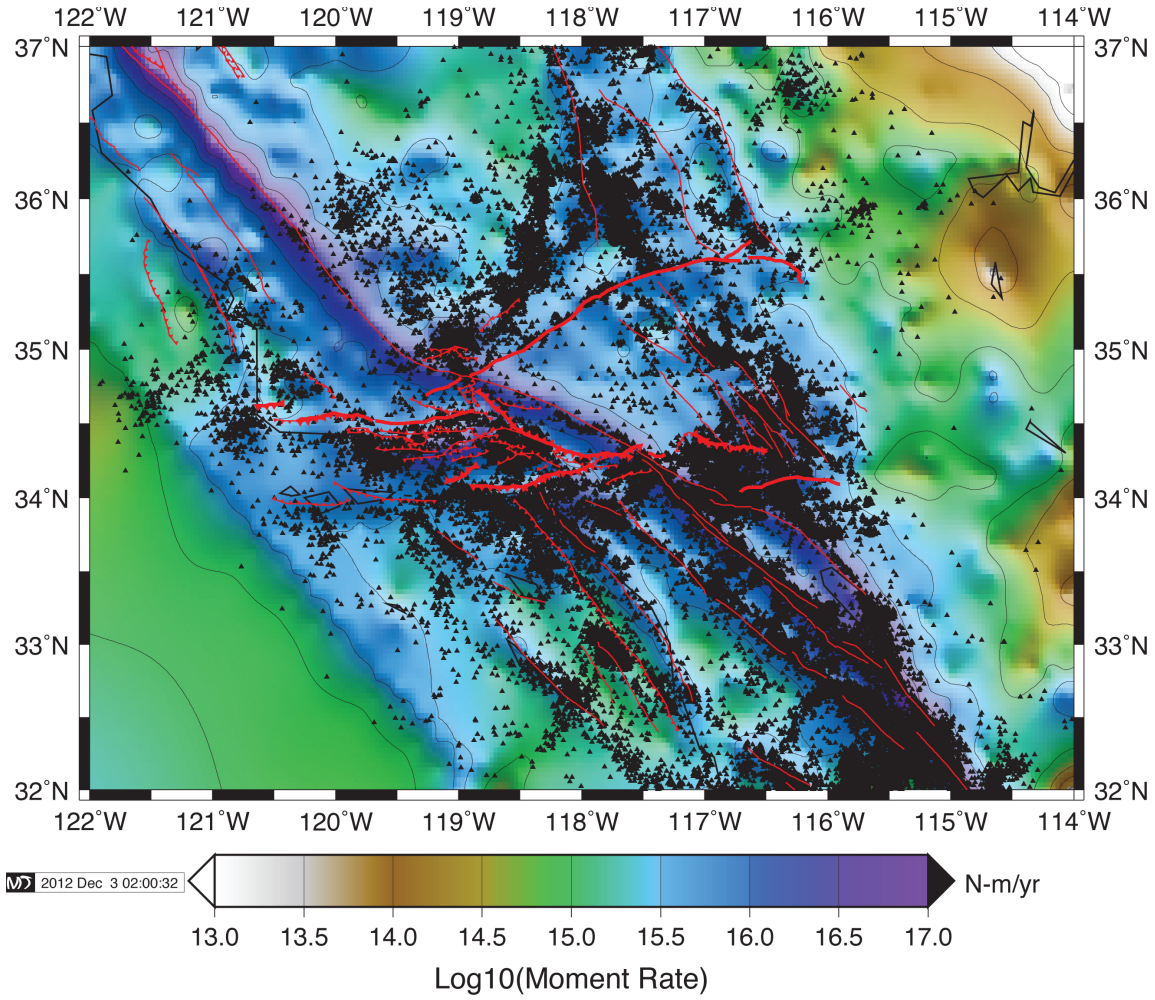

Figure 9. Total tectonic moment rate computed using equation 2 and the full horizontal velocity gradient tensor field obtained from UCERF3 GPS data. Black triangles represent the seismicity from the catalog since 1983.

Papers published with partial of full support from this USGS grant

Holt, W. E., and G. Shcherbenko (2013), Toward a Continuous Monitoring of the Horizontal Displacement Gradient Tensor Field in Southern California Using cGPS Observations from Plate Boundary Observatory (PBO), *Seism. Res. Lett.*, *vol. 84*, No. 3, doi: 10.1785/0220130004.

Papers fully supported by this grant in preparation that will be submitted by August, 2015:

Holt, W. E., The full horizontal velocity gradient tensor field in southern California obtained from the UCERF3 GPS velocity field, J. Geophys. Res., (in preparation for submission in August, 2015).

Holt, W. E., Ghosh, A., Chen, Yu, Using GPS Derived Shear Strain Rates in Southern California to Constrain Fault Slip Rate, Locking Depth, and Residual Off-Fault Strain Rates, (in preparation for submission in August, 2015).